



ARTICLE

A Symplectic Method of Numerical Simulation on Local Buckling for Cylindrical Long Shells under Axial Pulse Loads

Kecheng Li, Jianlong Qu, Jinqiang Tan, Zhanjun Wu and Xinsheng Xu*

State Key Laboratory of Structure Analysis for Industrial Equipment, Department of Engineering Mechanics, Dalian University of Technology, Dalian, 116024, China

*Corresponding Author: Xinsheng Xu. Email: xsxu@dlut.edu.cn

Received: 08 October 2020 Accepted: 20 November 2020

ABSTRACT

In this paper, the local buckling of cylindrical long shells is discussed under axial pulse loads in a Hamiltonian system. Using this system, critical loads and modes of buckling of shells are reduced to symplectic eigenvalues and eigensolutions respectively. By the symplectic method, the solution of the local buckling of shells can be employed to the expansion series of symplectic eigensolutions in this system. As a result, relationships between critical buckling loads and other factors, such as length of pulse load, thickness of shells and circumferential orders, have been achieved. At the same time, symmetric and unsymmetric buckling modes have been discuss. Moreover, numerical results show that modes of post-buckling of shells can be Bamboo node-type, bending type, concave type and so on. Research in this paper provides analytical supports for ultimate load prediction and buckling failure assessment of cylindrical long shells under local axial pulse loads.

KEYWORDS

Hamiltonian system; symplectic method; local buckling; buckling analysis; cylindrical long shell; axial pulse load

1 Introduction

Cylindrical long shell is a typical and classical structure in engineering, for example submarine pipelines, which are the core of marine oil and gas transportation [1]. In complex seabed environment, the long shell structures are more prone to instability because of ocean waves and/or currents, which is one of the main causes of structural failure [2,3]. The buckling problem of cylindrical shells has been noticed all along, and it is widely recognized that the sudden loss of capability of bending-bearing contributes to this kind of failure. More specifically speaking, the membrane stiffness is much higher than the bending stiffness for shell structures, at the beginning, external compression energy is absorbed through membrane deformation and stored as membrane strain energy, up to a point, this energy will be converted to bending strain energy, which leads to large deflection and complex bending deformation modes, and the buckling initiates. For a long shell structure, buckling usually occurs before material yielding, which could result in catastrophic consequences, hence, buckling load design is normally ahead of other kinds of strength design.

Generally, it is difficult to solve buckling problems theoretically, and therefore most research works concentrate upon experimental methods and numerical methods. At present, research trends on cylindrical



shell buckling focus more on accurate experiment techniques, advanced new materials, local buckling effects and micro scale structures, literatures on these areas are enormous. Wang et al. [4] implemented experiments to analyze geometrical imperfection sensitivity of cylindrical shells buckling. Fatma et al. [5] analyzed the effect of dent variation on buckling and post-buckling behaviors for cylindrical thin shells. Skukis et al. [6] proposed an experiment based vibration correlation technique to measure buckling loads of composite cylindrical shells. Experimental studies had shown that dynamic buckling modes of cylindrical shells could be mushroom-type and petal type under high speed impact [7]. In fact, the local buckling of cylindrical shells is mainly caused by uneven stress distribution. When subjected to an impact, stress wave continually compress the shell until transverse stiffness is not capable enough to sustain lateral shape, thus may cause local buckling of shells [8]. It is worth mentioning that experimentally achieved results are effective, but they are limited to too many experiment conditions, such as experiment facilities, specimen qualities, loading methods, dispersity of test samples and so on, and thus theoretical results are needed for necessary supplement in a full comprehension of shell buckling problems. Sun et al. [9] developed a method to solve buckling problems of piezoelectric cylindrical nanoshells using Eringen's nonlocal theory. Safarpour et al. [10] investigated buckling behavior for carbon nanotube reinforced cylindrical piezoelectric shell using a generalized differential quadrature method. In recent years, functionally graded multilayer structure is a hot topic on cylindrical shell buckling study, and many classical mathematical and mechanical methods have been applied to investigate instability of these structures [11–13]. Despite above aspects, the most commonly used method in shell buckling analysis now is finite element method (FEM), especially in engineering areas. With its simplicity and high efficiency, FEM has been applied to solve buckling problems for all kinds of cylindrical shells ranging from nano shells to macro shell structures [4,14]. Local characteristics of cylindrical shell buckling is of great practical meaning in shell buckling analysis, on that account, researchers have studied this problem with all kinds of techniques for a long time [15–17]. Anyhow, some researchers have proposed some theoretical methods to analyze the mechanism of traditional structural buckling [18–20], but they were lack of rigorous theoretical deductions for solving buckling governing equations and directly formulated experience based solutions, which might be incomplete. What's more, there's an insufficiency of study on cylindrical long shell's local buckling behaviors. And the very point that should be noted is that many works had been done on shell buckling problems using Ritz approximation, finite element codes, engineering estimation or other methods [21–28], which are all approximate solutions. However, great value can be achieved if theoretically accurate solutions to the buckling behaviors are given, by which the essence of its physical phenomena can be better understood.

Previous analytical methods mentioned are effective techniques for studying buckling of shells and are based upon the Lagrangian system. One of the mechanisms in common for these methods in solving high order partial differential governing equations is that their attentions are dedicated to approximate solutions, like inverse solutions and semi-inverse solutions. There's another system, i.e., the Hamiltonian system, it is a dual system that has been proved to be valid for decades and it is equivalent with Lagrangian system, in addition, it has been successfully applied on many fields, such as shell buckling, dynamics, wave propagation, vibration, fluid mechanics and so on [29]. The difference is that in Hamiltonian system it is easier to get a generalized solution in solving high order buckling governing equations using the method of separation of variables to reduce the order of equations in a complete form [30]. Based on advantage of the Hamiltonian system, some problems of pre-buckling of short shells are discussed [31–34]. In this paper, the local buckling problem of cylindrical long shells under pulse load is analyzed by the symplectic method without pre-assumed analytic shape functions. The solutions and results can give good predictions on ultimate loads and buckling modes development for long cylindrical shells with local compression loads, and may provide guidance for failure analysis and buckling resistance design for long shell structures.

2 The Fundamental Problem and Hamiltonian System

Consider an elastic circular cylindrical shell under axial pulse loads, in which its radius is R , thick h , Young's modulus E , Poisson's ratio ν and density ρ . The shell has infinite length and the length of compressive load N of axial pulse is $2l$. In the circular cylindrical coordinate (r, θ, x) as seen in Fig. 1. w is lateral displacement in the neutral surface along the r direction, and the boundary conditions can be expressed as

$$\begin{cases} w|_{x \rightarrow +\infty} = 0 \\ w|_{x \rightarrow -\infty} = 0 \end{cases} \quad (1)$$

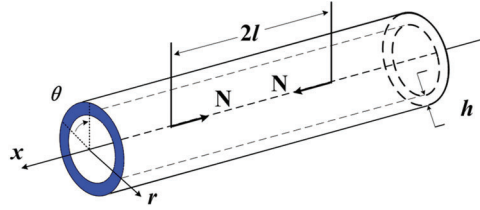


Figure 1: Coordinates and shell nomenclature

Based on the theory of the small deformation, the Lagrangian function (deformation energy) can be written as

$$\begin{aligned} L_e = & \frac{K}{2} \left(\frac{w}{R} \right)^2 + \frac{D}{2} \left[\left(\frac{\partial^2 w}{\partial x^2} \right)^2 + \frac{1}{R^2} \left(\frac{\partial^2 w}{\partial \theta^2} \right)^2 + \frac{2\nu}{R^2} \left(\frac{\partial^2 w}{\partial x^2} \right) \left(\frac{\partial^2 w}{\partial \theta^2} \right) \right. \\ & \left. + 2(1-\nu) \frac{1}{R^2} \left(\frac{\partial^2 w}{\partial x \partial \theta} \right)^2 \right] - \frac{N}{2} \left(\frac{\partial w}{\partial x} \right)^2 \end{aligned} \quad (2)$$

where $D = Eh^3/[12(1-\nu^2)]$ for bending stiffness, and $K = Eh/(1-\nu^2)$ for tensile stiffness.

The circular coordinate θ is taken in analogy to the time coordinate, and $\partial_\theta \equiv \partial/\partial\theta, \partial_x \equiv \partial/\partial x$. Introduce $\varphi = -\partial_\theta w/R$ representing circular twist angle, and denote $\dot{f} \equiv \partial_\theta f/R$. The dual variables of the original variables $\mathbf{q} = \{w, \varphi\}^T$ can be expressed as $\mathbf{p} = \{p_1, p_2\}^T$ where

$$\begin{cases} p_1 = -D(\partial_x^2 \dot{w} + \ddot{w}) \\ p_2 = -D(\partial_x^2 w - \dot{\varphi}) \end{cases} \quad (3)$$

p_1 and p_2 represent equivalent shear load and bending moment respectively. Then the Hamiltonian function is expressed in dual variables as

$$H(\mathbf{p}, \mathbf{q}) = \mathbf{p}^T \dot{\mathbf{q}} - L(\mathbf{p}, \mathbf{q}) \quad (4)$$

Introduce the state vector

$$\psi = \{w, \varphi, p_1, p_2\}^T = \{\mathbf{q}^T, \mathbf{p}^T\}^T \quad (5)$$

The dual equations of the Hamiltonian system can be rewritten in the form: $\dot{\mathbf{q}} = \delta H/\delta \mathbf{p}$ and $\dot{\mathbf{p}} = -\delta H/\delta \mathbf{q}$, namely

$$\dot{\psi} = \mathbf{H} \psi \quad (6)$$

\mathbf{H} is a Hamiltonian operator matrix, and has the expression

$$\mathbf{H} = \begin{bmatrix} 0 & -1 & 0 & 0 \\ \partial_x^2 & 0 & 0 & 1/D \\ K + N\partial_x^2 & 0 & 0 & -\partial_x^2 \\ 0 & 0 & 1 & 0 \end{bmatrix} \quad (7)$$

The dual equations in Hamiltonian system are equivalent with the governing equations in Lagrangian system, but they will be solved in a symplectic space.

3 Symplectic Eigenvalues and Eigensolutions

In symplectic system, the method of separation of variables can be used. The solution of Eq. (6) can be uniformly written as $\psi = \psi_\mu e^{i\mu\theta}$, where μ is symplectic eigenvalue [29]. According to the closed conditions of cylindrical shells, the solution satisfies the continuity condition in circumferential direction

$$\psi|_{\theta=0} = \psi|_{\theta=2\pi} \quad (8)$$

Therefore, the eigenvalues in circumferential direction are

$$\mu_n = in (n = 0, \pm 1, \pm 2, \dots) \quad (9)$$

where the eigensolutions of $\mu_0 = 0$ and $\mu_n \neq 0$ correspond to the axisymmetric and non-axisymmetric buckling problems, respectively.

The complete solutions of the original problem can be expressed as

$$\psi^{(n)} = \begin{cases} \psi_1^{(n)} = [C_5\kappa_5 e^{\lambda_3 x} + C_6\kappa_6 e^{\lambda_4 x}] e^{in\theta} & (x < -l) \\ \psi_2^{(n)} = [C_1\kappa_1 e^{\lambda_1 x} + C_2\kappa_2 e^{-\lambda_1 x} + C_3\kappa_3 e^{\lambda_2 x} + C_4\kappa_4 e^{-\lambda_2 x}] e^{in\theta} & (-l \leq x \leq l) \\ \psi_3^{(n)} = [C_7\kappa_7 e^{-\lambda_3 x} + C_8\kappa_8 e^{-\lambda_4 x}] e^{in\theta} & (x > l) \end{cases} \quad (10)$$

where C_k ($k = 1, 2, \dots, 8$) is undetermined constant, and λ is the eigensolution in axial direction, namely

$$\begin{cases} \lambda_{1,2} = i\{(NR^2/2D - n^2) \mp [(NR^2/2D - n^2)^2 - \gamma_n]^{1/2}\}^{1/2}/R \\ \lambda_{3,4} = \gamma_n^{1/4}\{[1 - n^2/\gamma_n^{1/2}]^{1/2} \pm i[1 + n^2/\gamma_n^{1/2}]^{1/2}\}/\sqrt{2}R \end{cases} \quad (11)$$

γ_n is intermediate coefficient related with n , which can be expressed as $\gamma_n = n^4 + KR^2/D$, and constant vectors, κ_k ($k = 1, 2, \dots, 8$), can be shown as

$$\begin{cases} \kappa_1 = \kappa_2 = \{1, -in/R, -Din(\lambda_1^2 R^2 - n^2)/R^3, -D(\lambda_1^2 R^2 - n^2)/R^2\}^T \\ \kappa_3 = \kappa_4 = \{1, -in/R, -Din(\lambda_2^2 R^2 - n^2)/R^3, -D(\lambda_2^2 R^2 - n^2)/R^2\}^T \\ \kappa_5 = \kappa_7 = \{1, -in/R, -Din(\lambda_3^2 R^2 - n^2)/R^3, -D(\lambda_3^2 R^2 - n^2)/R^2\}^T \\ \kappa_6 = \kappa_8 = \{1, -in/R, -Din(\lambda_4^2 R^2 - n^2)/R^3, -D(\lambda_4^2 R^2 - n^2)/R^2\}^T \end{cases} \quad (12)$$

4 Critical Loads and Buckling Modes

For piecewise eigensolution (10), continuity conditions can be expressed as

$$\begin{cases} \mathbf{D}_1 \psi_1^{(n)}|_{x=-l} = \mathbf{D}_2 \psi_2^{(n)}|_{x=-l} \\ \mathbf{D}_3 \psi_3^{(n)}|_{x=l} = \mathbf{D}_2 \psi_2^{(n)}|_{x=l} \end{cases} \quad (13)$$

where operator matrices $\mathbf{D}_k = [\mathbf{d}_k, \mathbf{0}, \mathbf{0}, \mathbf{d}_4]$ ($k = 1, 2, 3$), operator vectors $\mathbf{d}_1 = \mathbf{d}_3 = \{1, \partial_x, 0, 0\}^T$, $\mathbf{d}_2 = \{1, \partial_x, 0, N\partial_x\}^T$ and $\mathbf{d}_4 = \{0, 0, 1, \partial_x\}^T$. Since eigensolution (10) should satisfy continuity

conditions (13), the undetermined constants C_1, C_2, \dots, C_8 and critical loads can be determined. Namely eight algebraic equations can be rewritten by conditions (13) as

$$\mathbf{B}\mathbf{c} = 0 \quad (14)$$

where $\mathbf{c} = \{C_1, C_2, \dots, C_8\}^T$. If \mathbf{c} is nonzero vector, there is a buckling mode at least. Therefore, the bifurcation condition is that the determinant of the coefficients equals to zero, or

$$|\mathbf{B}| = 0 \quad (15)$$

The critical loads and the corresponding buckling modes can be determined by Eqs. (10), (13) and (14). It should be noted that critical load has many roots from Eq. (14) for a fixed n , so denote m ($m = 1, 2, \dots$) and n ($n = 0, 1, 2, \dots$) as the axial order and circumferential order of the shell buckling. Rewrite the eigensolution (10) as $\psi_{nm}^{(\alpha)}(X)e^{in\theta}$ for n and $\psi_{nm}^{(\beta)}(X)e^{-in\theta}$ for $-n$ while $n \neq 0$. For $n = 0$, $\psi_{0m}^{(\beta)}(X, \theta)$ is the Jordan form of $\psi_{0m}^{(\alpha)}(X)$. Introduce the inner product of the function as

$$\langle \psi_1, \psi_2 \rangle = \int_{-\infty}^{-L} \int_0^{2\pi} \psi_1^T \mathbf{J} \psi_2 d\theta dX + \int_{-L}^L \int_0^{2\pi} \psi_1^T \mathbf{J} \psi_2 d\theta dX + \int_L^{\infty} \int_0^{2\pi} \psi_1^T \mathbf{J} \psi_2 d\theta dX \quad (16)$$

where \mathbf{J} is a unit rotational matrix [29]. By orthogonalizing, it can be proved that there are adjoint symplectic orthogonal relations between the eigensolutions as following

$$\begin{cases} \langle \psi_{nm}^{(\alpha)}(X, \theta), \psi_{kj}^{(\beta)}(X, \theta) \rangle = -\langle \psi_{nm}^{(\beta)}(X, \theta), \psi_{kj}^{(\alpha)}(X, \theta) \rangle = \delta_n \delta_k \delta_m \delta_j \\ \langle \psi_{nm}^{(\alpha)}(X, \theta), \psi_{kj}^{(\alpha)}(X, \theta) \rangle = \langle \psi_{nm}^{(\beta)}(X, \theta), \psi_{kj}^{(\beta)}(X, \theta) \rangle = 0 \end{cases} \quad (17)$$

Since the symplectic space is complete, the mode of buckling can be obtained by expanding the eigensolutions (10) as

$$\psi = \sum_{n,m=1}^{\infty} [A_{nm}\psi_{nm}^{(\alpha)}(X)e^{in\theta} + B_{nm}\psi_{nm}^{(\beta)}(X)e^{-in\theta}] + \sum_{m=1}^{\infty} C_m\psi_{0m}^{(\alpha)}(X) \quad (18)$$

where the unknown coefficients, A_{nm} , B_{nm} and C_m , can be determined from boundary conditions.

5 Numerical Results

For simplicity, define the following dimensionless terms: $X = x/R$, $W = w/R$, $L = l/R$, $H = h/R$, $N_{cr} = NR^2/D$ and $\gamma = KR^2/D$. Consider an infinite elastic circular cylindrical shell with Poisson's ratio $\nu = 0.25$ and $H = 0.01$. Numerical results are discussed below.

As the first example, take L from 0.1 to 1, the relationship between critical loads of the first five orders and the length of axial load is depicted in Fig. 2. The figures show downward trends of critical loads with the length for $n = 0, 1, 2, 3$ and $m = 1, 2, 3, 4, 5$. For branches m with odd numbers, the trends are nonmonotonic decreasing, for m with the even numbers, the trends are basically monotonic decreasing. From this result we can see the complexity of buckling problem and difference between axisymmetric buckling behaviors and non-axisymmetric behaviors. What's more, the curve patterns are nearly the same for a specific m with different n on the whole. Another interesting point is that the critical loads have similar values for a specific n with different m , which illustrates that buckling modes can be various while the critical loads are similar. For given loading length and circumferential order n , the critical load becomes higher while the branch order m increases, the reason for this is that the more complex the buckling mode is the more energy or larger load is needed. Furthermore, there are limit loads when the length L becomes infinite, but the influence of loading length is different for each m , in the large, the higher the m becomes, the bigger the length value is when the curve approaches smooth.

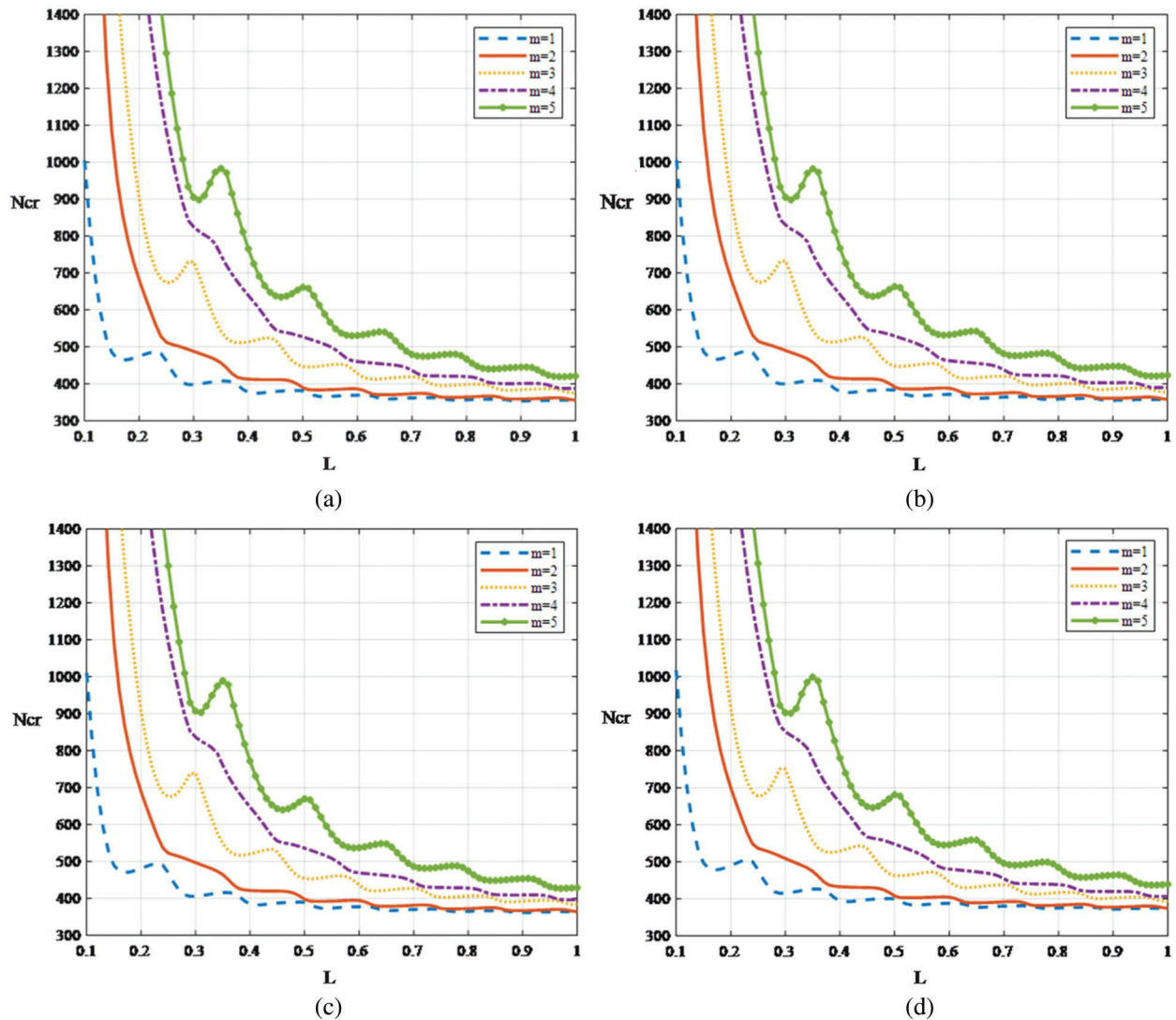


Figure 2: The relationship between critical loads and the length of axial load for $n = 0,1,2,3$. (a) $n = 1$, (b) $n = 1$, (c) $n = 2$ and (d) $n = 3$

To reveal the internal law of buckling with respect to circumferential orders n , Fig. 3 gives the curves of critical loads for the first ten circumferential orders n . The results shows that the higher the order n is the higher the critical load becomes, and it is more obvious for higher orders. The critical loads present a wave trend for a given n , and then become gentle as length of axial load increases, and finally reach stable values. With the form of eigensolutions in (7), it is easy to find that there are infinite theoretical solutions for every n , however, only the top-ranking solutions are of great importance, especially the first one which is also the lowest and usually occurs the first. While the length of axial load is small, particularly when $L < 0.1$, critical loads for different n are very close, with which some experimental phenomena can be illustrated, for example, sometimes several buckling modes of a short shell can coexist in one specimen, and in some other cases, the first buckling mode of the same batch of specimen can be different. As the length of loading area grows, particularly when $L > 0.3$, the critical loads are distinctly separated for different order n .

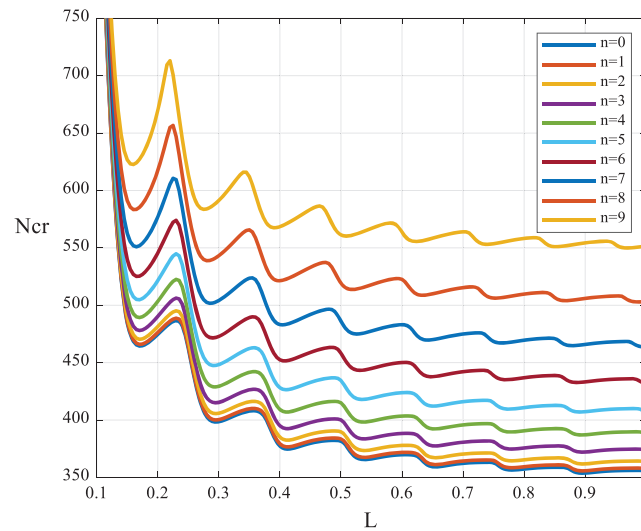


Figure 3: The curves of critical loads for the first ten circumferential orders n

The buckling modes are shown in Figs. 4–7, which correspond to buckling modes for circumferential orders $n = 0, 1, 2, 3$ when $L = 0.1$, and the first five axial orders $m = 1, 2, 3, 4, 5$ are chosen in particular. It is obvious that Fig. 4 gives axisymmetric buckling modes when $n = 0$, and the number of circumferential waves is 0. The shape of the buckling region is similar to bamboo node, and some researchers call it bamboo node-type buckling. Moreover, as the axial branch number m grows, in other words, as the axial load increases, the number of axial waves goes up. Even though the taken $L = 0.1$ is relatively small, it is still easy to recognize the axial wave mode when $m < 5$ in Fig. 4, which would be a problem in FEM simulations since element size may be larger than the axial wave distance. For engineering cylindrical structures under axial compression, the bamboo node-type mode is the most common seen buckling form.

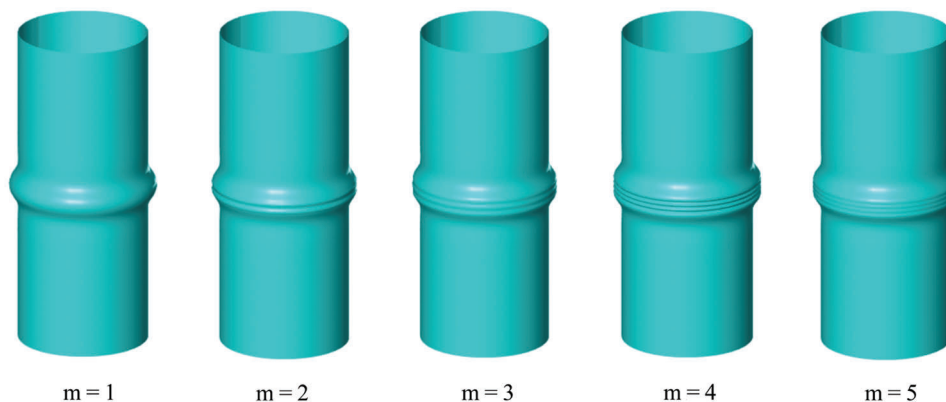


Figure 4: Shell buckling modes of the first 5 branches with circumferential order $n = 0$

Fig. 5 shows anti-symmetrical buckling modes for $n = 1$ with $m = 1, 2, 3, 4, 5$. The number of circumferential waves is 1, and the axial wave number also goes up along with increasing of m . The shape of the buckling region is similar to a bending tube, thus some researchers call it bending type buckling. This type of mode is also a common buckling mode in cylindrical long shell structures, especially for that with local defects.

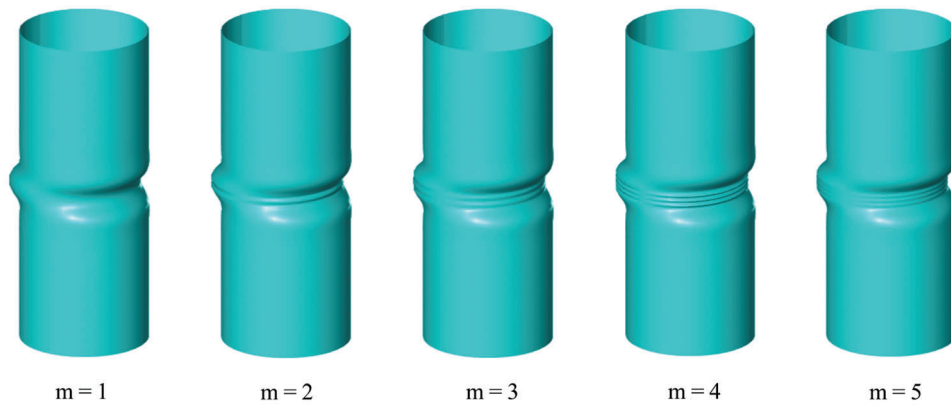


Figure 5: Shell buckling modes of the first 5 branches with circumferential order $n = 1$

Figs. 6 and 7 show higher order buckling modes for $n = 2$ and $n = 3$ with $m = 1, 2, 3, 4, 5$. Their circumferential wave numbers are 2 and 3, respectively. The increasing of number of buckling waves has similar law with cases above. The shape of the buckling region is similar to periodically arranged concaves, thus some researchers call the buckling modes of $n \geq 2$ concave type buckling. These kinds of buckling often occur in anisotropic material shells. Specially, the circumferential mode for $n = 2$ is orthogonally symmetric.

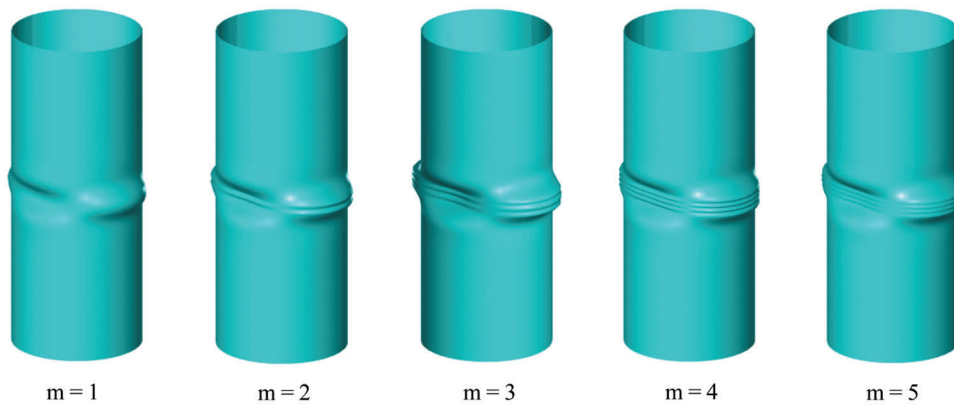


Figure 6: Shell buckling modes of the first 5 branches with circumferential order $n = 2$

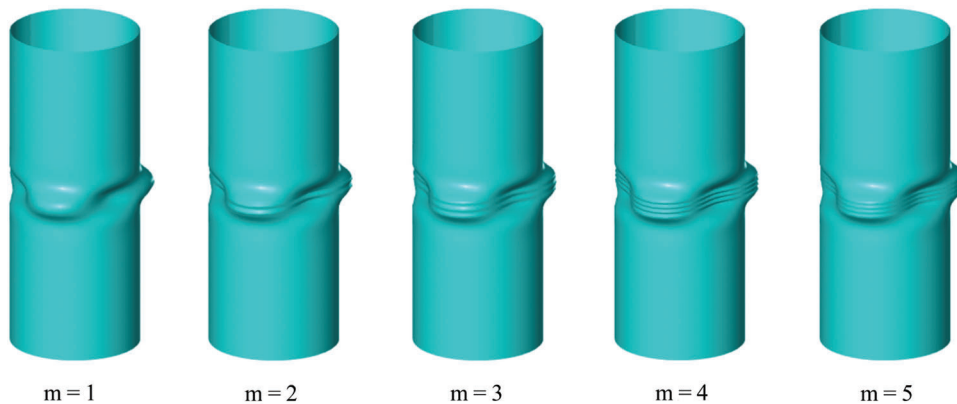


Figure 7: Shell buckling modes of the first 5 branches with circumferential order $n = 3$

Take $L = 0.11$, Fig. 8 gives the first branch buckling modes of shells for circumferential orders $n = 0-9$. The result indicates that the circumferential wave numbers match the circumferential orders and high order buckling modes display more complicated deformation shapes. The figures also demonstrate that the buckling modes evolve from simple bamboo node-type to bending type and concave types, which correspond to mode characteristics of buckling states of $n = 0$, $n = 1$ and $n \geq 2$, respectively. All these modes exhibit characteristics of locality.

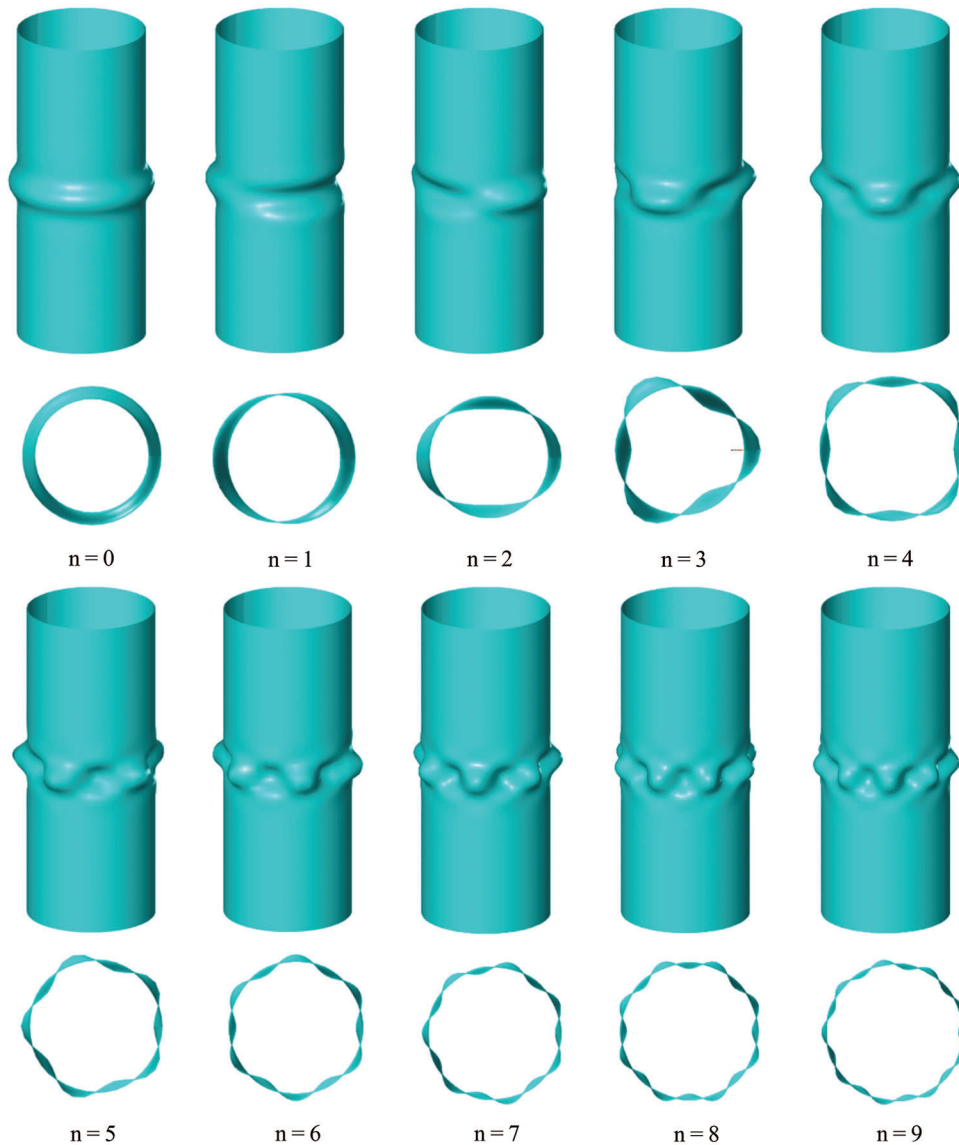


Figure 8: Buckling modes of shells for circumferential order n from 0 to 9

Take the axisymmetric buckling mode ($n = 0$) and the first bifurcation mode ($m = 1$) for example to study the influence of length of axial load. And buckling modes for loading length $L = 0.1, 0.2, \dots, 1.0$ are plotted in Fig. 9, respectively. From the images, it is obvious to see that buckling wrinkles located in the region where axial load is applied, and thus the number of the axial wrinkle waves increases with the scale of loading area. It should be noted

that the number of axial wrinkles waves does not increase linearly with the length of axial load on account of the significant influence of material properties. To investigate the evolution pattern of the wrinkle waves in axial direction, numbers of axial wrinkle waves are listed in Tab. 1 for different kinds of buckling modes.

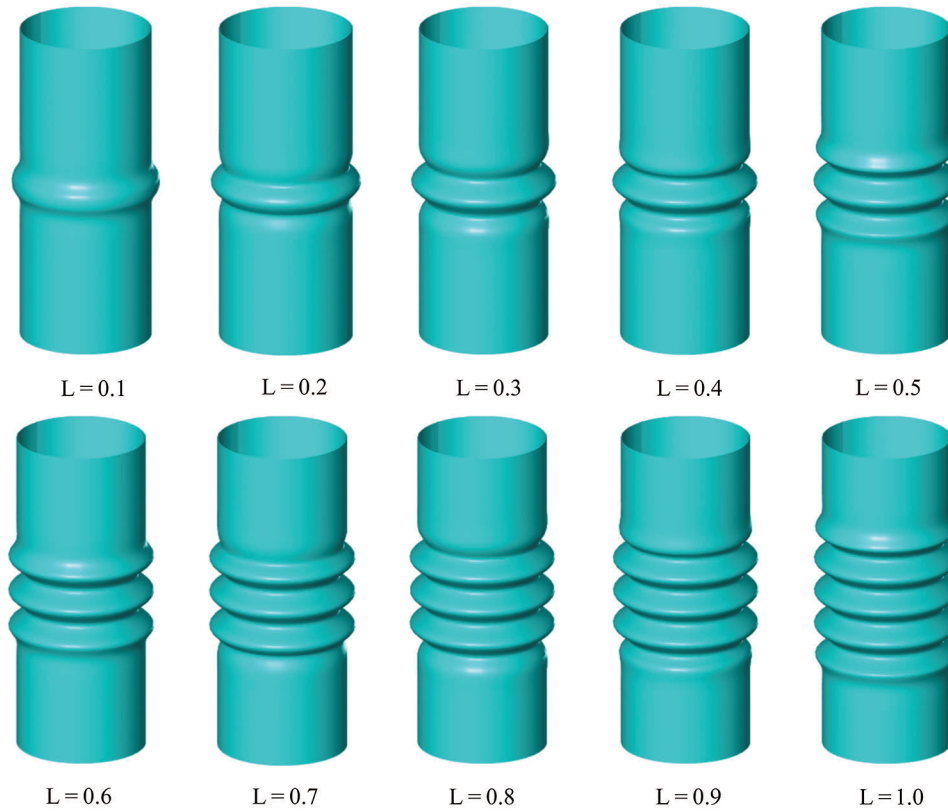


Figure 9: Buckling modes of shells with length of load from 0.1 to 1.0

Table 1: Number of axial wrinkle waves for different length of load region

L	$n = 0$	$n = 1$	$n = 2$	$n = 3$
0.1	1	1	1	1
0.2	1	3	3	3
0.3	2	3	3	3
0.4	2	5	5	5
0.5	3	5	5	5
0.6	3	5	5	5
0.7	3	7	7	7
0.8	3	7	7	7
0.9	4	9	9	9
1.0	4	9	9	9

As seen in Tab. 1, the number of axial wrinkle waves are positively correlated with the length of axial load. In cases that L is small, such as $L \leq 0.1$, the axial wrinkle wave number is always 1 for different n . As the L increases, it gets easier for the shells to buckle, accordingly, the axial wrinkle wave number goes up. And it is not difficult to conclude from the data that the axial wrinkle number grows in a natural order in the axial symmetric buckling cases and grows in an odd sequence order in the non-symmetric buckling cases. This conclusion can be useful for prediction of collapsing modes for cylindrical thin shells and helpful for geometry and loading design of cylindrical shell structures.

To discuss the thickness effect, define another dimensionless critical load, $P_{cr} = N/ER$, which is independent of thickness, while the dimensionless load $N_{cr} = NR^2/D$ has something to do with thickness. In fact, the relationship between P_{cr} and N_{cr} can be expressed as $N_{cr}H^3 = 12(1-\nu^2)P_{cr}$. Take the critical load of bending type buckling ($n = 1$) as an example, Fig. 10 illustrates the relation of critical loads with thickness of shells from two perspectives. Fig. 10a presents the curves of critical load P_{cr} and the length of load L with 5 different thickness values, which indicates that the critical loads decrease with the length of load in a non-monotonic way, the critical load curves drop sharply when $L < 0.2$, and vary smoothly when $L > 0.2$, and finally approach flat. Fig. 10b presents P_{cr} and the shell thickness with four different length of load, which depicts that the critical loads increase with growth of shell thickness in a monotonic way. What's more, the trend of the curves varies from a quadratic type to a linear type when the length of load grows. Further, load curve for $L = 0.1$ is much higher than the other curves, and load curves for $L = 0.2, 0.4, 0.5$ are quite close, from which we can obtain that buckling mode of a very short shell needs quite big energy or compressive load to arouse, when the length grows to a critical value, the buckling load will sharply decrease and the buckling deformation becomes more easily.

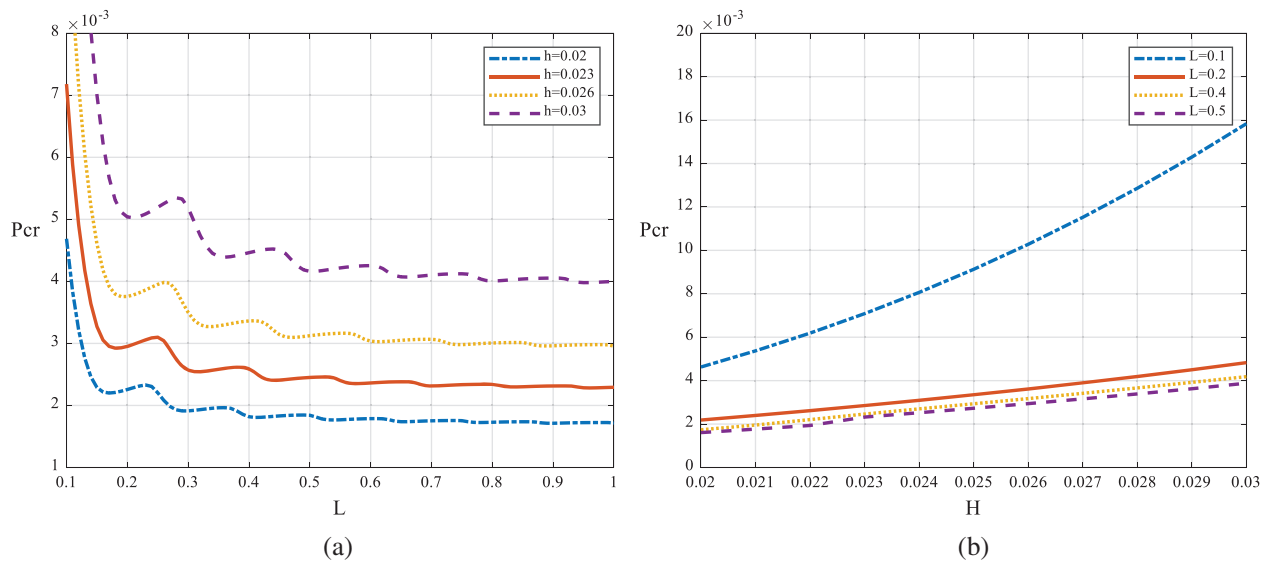


Figure 10: Critical loads with pulse length and thickness of shells when $n = 1$. (a) P_{cr} vs. normalized length of load and (b) P_{cr} vs. normalized thickness

6 Solution Verification by Comparison with FEM Results

To verify the effectiveness of the method used for buckling prediction above, a comparison between the FEM results and the results of this paper are implemented. In the FEM simulation an infinite long cylindrical shell is simplified to a finite long shell with $L/R = 20$, and set the $R = 1$, $H = 0.01$, $E = 200$ GPa, $\nu = 0.25$. The ends of the shell are far enough from the loading region, so that end boundary conditions hardly effect the local buckling in the middle region, and then set the end boundary conditions to be simply supported. Set the

ends of the loading region to be free of external constraints, and only exert a pair of axial compressive loads. 3 FEM models were established, in which 3 values of the length of loading region were taken: $L = 0.6 R$, $L = 0.8 R$, and $L = 1 R$. Due to the mesh size effect, the length of the mesh was taken to be 0.1, which is small enough to get accurate results. The overall mesh quantity is 12600. A 4-node doubly curved thin shell mesh strategy was adopted with reduced integration and hourglass control. The FEM model is shown in Fig. 11.

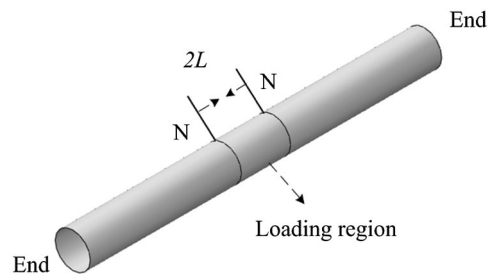


Figure 11: FEM model of cylindrical long shell

The generalized critical buckling load of the first branch for each FEM model is employed in contrast to the results in this paper as shown in Tab. 2 below. From the statistics in Tab. 2, we can see that the results in this paper are consistent with FEM results, and the results are more accordant for the cases in which L is large.

Table 2: Critical buckling loads of results from FEM and present method

L	$L = 0.6 R$	$L = 0.8 R$	$L = 1 R$
Ncr/FEM	369.77	355.87	354.69
Ncr/Present	381.87	363.23	355.86

Corresponding to Figs. 12a and 12b, the selected cylindrical shell buckling patterns are the same for FEM and present results, and thus the reliability and accuracy are verified.

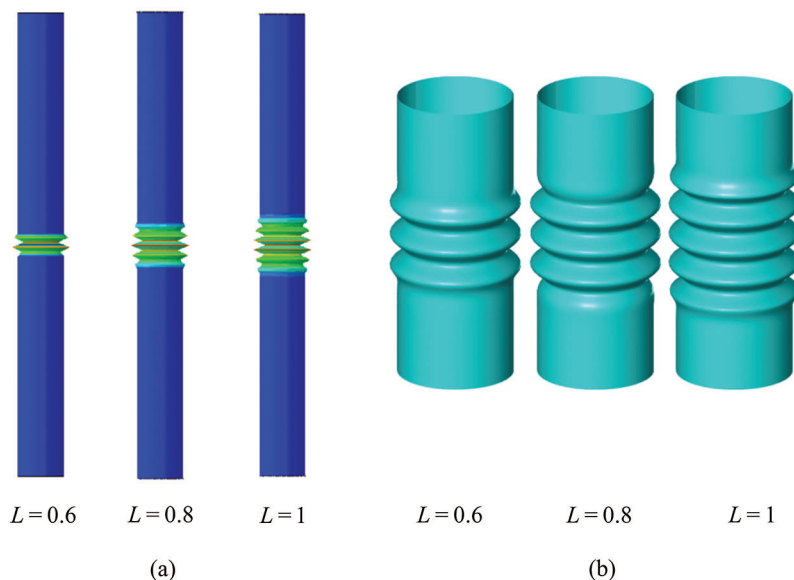


Figure 12: Shell buckling modes for FEM and present results when $L = 0.6, 0.8, 1$. (a) FEM results and (b) Present results

7 Conclusions

In Hamiltonian system, critical loads and modes of buckling of long shells are reduced to symplectic generalized eigenvalues and eigensolutions respectively. Under axial pulse loads, buckling of cylindrical long shells may happen and the main reason for the local buckling of shells is the pulse load. The critical load of local buckling of long shells is related to material constants and geometric parameters of shells and the pulse length of loads. The eigensolutions, modes of local buckling of shells, can be expressed by two parameters, namely axial order m and circumferential order n of buckling modes. The modes corresponding to these parameters show special phenomena. Eigensolutions of the zero eigenvalue represent the axisymmetric buckling modes and eigensolutions of the non-zero eigenvalues represent non-axisymmetric modes. The number of wrinkles along axial and circumferential directions and the buckling types depend on the parameters n and m . Numerical analysis reveals that the modes of local buckling of long shells mainly include bamboo node-type modes ($n = 0$), bending type modes ($n = 1$), concave type buckling modes ($n \geq 2$) and so on. Results from this paper show good agreement with FEM results, and thus the reliability of the methodology imposed in this paper is verified. The symplectic method can also provide an analytical support to solve the problem of post-buckling of shells.

Funding Statement: This research is funded by the grants from Dalian Project of Innovation Foundation of Science and Technology (No. 2018J11CY005) and Research Program of State Key Laboratory of Structural Analysis for Industrial Equipment (No. S18313).

Conflicts of Interest: The authors declare that they have no conflicts of interest to report regarding the present study.

References

1. Jiang, F. Y., Dong, S., Zhao, Y. L., Xie, Z. X., Guedes Soares, C. G. (2019). Investigation on the deformation response of submarine pipelines subjected to impact loads by dropped objects. *Ocean Engineering*, 194(106638), 1–18. DOI 10.1016/j.oceaneng.2019.106638.
2. Li, X. H., Chen, G. M., Zhu, H. W., Zhang, R. R. (2017). Quantitative risk assessment of submarine pipeline instability. *Journal of Loss Prevention in the Process Industries*, 45(7), 108–115. DOI 10.1016/j.jlp.2016.12.001.
3. Gao, F. P. (2017). Flow-pipe-soil coupling mechanisms and predictions for submarine pipeline instability. *Journal of Hydrodynamics*, 29(5), 763–773. DOI 10.1016/S1001-6058(16)60787-4.
4. Wang, B., Zhu, S. Y., Hao, P., Bi, X. J., Du, K. F. et al. (2018). Buckling of quasi-perfect cylindrical shell under axial compression: A combined experimental and numerical investigation. *International Journal of Solids and Structures*, 130–131(7), 232–247. DOI 10.1016/j.ijsolstr.2017.09.029.
5. Korucuk, F. M. A., Maali, M., Kilic, M., Aydin, A. C. (2019). Experimental analysis of the effect of dent variation on the buckling capacity of thin-walled cylindrical shells. *Thin-Walled Structures*, 143, 1–13.
6. Skukis, E., Ozolins, O., Kalnins, K., Arbelo, M. A. (2017). Experimental test for estimation of buckling load on unstiffened cylindrical shells by vibration correlation technique. *Procedia Engineering*, 172(8), 1023–1030. DOI 10.1016/j.proeng.2017.02.154.
7. Wang, B., Lu, G. (2002). Mushrooming of circular tubes under dynamic axial loading. *Thin-Walled Structures*, 40(2), 167–182. DOI 10.1016/S0263-8231(01)00057-X.
8. Xu, X. S., Zhang, G., Zeng, Q. C., Chu, H. J. (2011). Bamboo node-type local buckling of cylindrical shells under axial impact. *Advances in Vibration Engineering*, 10(1), 41–52.
9. Sun, J. B., Wang, Z. Y., Zhou, Z. H., Xu, X. S., Lim, C. W. (2018). Surface effects on the buckling behaviors of piezoelectric cylindrical nanoshells using nonlocal continuum model. *Applied Mathematical Modelling*, 59(4), 341–356. DOI 10.1016/j.apm.2018.01.032.
10. Safarpour, H., Ghanbari, B., Ghadiri, M. (2019). Buckling and free vibration analysis of high speed rotating carbon nanotube reinforced cylindrical piezoelectric shell. *Applied Mathematical Modelling*, 65(1), 428–442. DOI 10.1016/j.apm.2018.08.028.

11. Ansari, R., Gholami, R., Norouzzadeh, A. (2016). Size-dependent thermo-mechanical vibration and instability of conveying fluid functionally graded nanoshells based on mindlin's strain gradient theory. *Thin-Walled Structures*, 105, 172–184. DOI 10.1016/j.tws.2016.04.009.
12. Sahmani, S., Aghdam, M. M. (2017). Nonlinear instability of axially loaded functionally graded multilayer graphene platelet-reinforced nanoshells based on nonlocal strain gradient elasticity theory. *International Journal of Mechanical Sciences*, 131, 95–106. DOI 10.1016/j.ijmecsci.2017.06.052.
13. Trabelsi, S., Frikha, A., Zghal, S., Dammak, F. (2018). Thermal post-buckling analysis of functionally graded material structures using a modified FSDT. *International Journal of Mechanical Sciences*, 144, 74–89. DOI 10.1016/j.ijmecsci.2018.05.033.
14. Wang, Y., Feng, C., Zhao, Z., Yang, J. (2018). Buckling of graphene platelet reinforced composite cylindrical shell with cutout. *International Journal of Structural Stability & Dynamics*, 18(3), 1–17.
15. Seide, P., Weingarten, V. I., Hagemann, G., Alting, J., Preclik, D. et al. (1971). Effect of a local axisymmetric imperfection on the buckling behavior of a circular cylindrical shell under axial compression. *AIAA Journal*, 9(1), 48–52. DOI 10.2514/3.6123.
16. Krasovsky, V., Marchenko, V., Schmidt, R. (2011). Deformation and buckling of axially compressed cylindrical shells with local loads in numerical simulation and experiments. *Thin-Walled Structures*, 49(5), 576–580. DOI 10.1016/j.tws.2010.09.009.
17. Evkin, A., Krasovsky, V., Lykhachova, O., Marchenko, V. (2019). Local buckling of axially compressed cylindrical shells with different boundary conditions. *Thin-Walled Structures*, 141(8), 374–388. DOI 10.1016/j.tws.2019.04.039.
18. Nobile, L., Carloni, C. (2006). Buckling analysis of eccentrically loaded cracked columns. *Structural Durability & Health Monitoring*, 2(2), 83–90.
19. Obodan, N. I., Adlutskii, V. Y., Gromov, V. A. (2017). Vulnerability assessment of loaded thin-walled shells under an external pulse action. *Strength of Materials*, 49(2), 335–342. DOI 10.1007/s11223-017-9873-5.
20. Yadav, K. K., Gerasimidis, S. (2019). Instability of thin steel cylindrical shells under bending. *Thin Walled Structures*, 137(1), 151–166. DOI 10.1016/j.tws.2018.12.043.
21. Salahshour, S., Fallah, F. (2017). Elastic collapse of thin long cylindrical shells under external pressure. *Thin-Walled Structures*, 124(19), 81–87. DOI 10.1016/j.tws.2017.11.058.
22. Xue, J. (2012). Local buckling in infinitely, long cylindrical shells subjected uniform external pressure. *Thin-Walled Structures*, 53(10), 211–216. DOI 10.1016/j.tws.2012.01.008.
23. Som, P., Deb, A. (2014). A generalized Ritz-based method for nonlinear buckling of thin cylindrical shells. *Thin-Walled Structures*, 76, 14–27. DOI 10.1016/j.tws.2013.09.024.
24. Han, J. H., Kardomateas, G. A., Simitse, G. J. (2004). Elasticity, shell theory and finite element results for the buckling of long sandwich cylindrical shells under external pressure. *Composites Part B: Engineering*, 35(6–8), 591–598. DOI 10.1016/j.compositesb.2003.07.002.
25. Rahman, T., Jansen, E. L. (2010). Finite element based coupled mode initial post-buckling analysis of a composite cylindrical shell. *Thin-Walled Structures*, 48(1), 25–32. DOI 10.1016/j.tws.2009.08.003.
26. Lord, G. J., Champneys, A. R., Hunt, G. W. (1997). Computation of localized post buckling in long axially compressed cylindrical shells. *Localization and Solitary Waves in Solid Mechanics*, 355, 2137–2150.
27. Hunt, G. W., Neto, E. L. (1991). Localized buckling in long axially-loaded cylindrical shells. *Journal of the Mechanics and Physics of Solids*, 39(7), 881–894. DOI 10.1016/0022-5096(91)90010-L.
28. Stephens, B. W., Starnes, J. H. (1974). Collapse of long cylindrical shells under combined bending and pressure loads. *AIAA Journal*, 13(1), 20–25. DOI 10.2514/3.49624.
29. Lim, C. W., Xu, X. S. (2010). Symplectic elasticity: Theory and applications. *Applied Mechanics Reviews*, 63(050802), 1–10. DOI 10.1115/1.4003700.
30. Sun, J. B., Xu, X. S., Lim, C. W., Qiao, W. (2015). Accurate buckling analysis for shear deformable FGM cylindrical shells under axial compression and thermal loads. *Composite Structures*, 123(9), 246–256. DOI 10.1016/j.compstruct.2014.12.030.

31. Xu, X., Ma, Y., Lim, C. W., Chu, H. (2006). Dynamic buckling of cylindrical shells subject to an axial impact in a symplectic system. *International Journal of Solids and Structures*, 43(13), 3905–3919. DOI 10.1016/j.ijsolstr.2005.03.005.
32. Xu, X., Ma, J., Lim, C. W., Chu, H. (2009). Dynamic local and global buckling of cylindrical shells under axial impact. *Engineering Structures*, 31(5), 1132–1140. DOI 10.1016/j.engstruct.2009.01.009.
33. Sun, J. B., Xu, X. S., Lim, C. W. (2016). Combined load buckling for cylindrical shells based on a symplectic elasticity approach. *Journal of Theoretical and Applied Mechanics*, 54(3), 705–716.
34. Ni, Y. W., Tong, Z. Z., Rong, D. L., Zhou, Z. H., Xu, X. S. (2018). Accurate thermal buckling analysis of functionally graded orthotropic cylindrical shells under the symplectic framework. *Thin-Walled Structures*, 129, 1–9. DOI 10.1016/j.tws.2018.03.030.